JACS Au
AN OPEN ACCESS JOURNAL OF THE AMERICAN CHEMICAL SOCIETY

pubs.acs.org/jacsau

Article

Orientational Coupling of Molecules at Interfaces Revealed by Two-Dimensional Electronic−Vibrational Sum Frequency Generation (2D-EVSFG)

Zhi-Chao Huang-Fu,[§] Yuqin Qian,[§] Tong Zhang, Gang-Hua Deng, Jesse B. Brown, Haley Fisher, Sydney Schmidt, Hanning Chen, and Yi Rao*

Cite This: *JACS Au* 2023, 3, 1413−1423

Read Online

ACCESS | Metrics & More | Article Recommendations | Supporting Information

ABSTRACT: Photoinduced relaxation processes at interfaces are intimately related to many fields such as solar energy conversion, photocatalysis, and photosynthesis. Vibronic coupling plays a key role in the fundamental steps of the interface-related photoinduced relaxation processes. Vibronic coupling at interfaces is expected to be different from that in bulk due to the unique environment. However, vibronic coupling at interfaces has not been well understood due to the lack of experimental tools. We have recently developed a two-dimensional electronic−vibrational sum frequency generation (2D-EVSFG) for vibronic coupling at interfaces. In this work, we present orientational correlations in vibronic couplings of electronic and vibrational transition dipoles as well as the structural evolution of photoinduced excited states of molecules at interfaces with the 2D-EVSFG technique. We used malachite green molecules at the air/water interface as an example, to be compared with those in bulk revealed by 2D-EV. Together with polarized VSFG and ESHG experiments, polarized 2D-EVSFG spectra were used to extract relative orientations of an electronic transition dipole and vibrational transition dipoles at the interface. Combined with molecular dynamics calculations, time-dependent 2D-EVSFG data have demonstrated that structural evolutions of photoinduced excited states at the interface have different behaviors than those in bulk. Our results showed that photoexcitation leads to intramolecular charge transfer but no conical interactions in 25 ps. Restricted environment and orientational orderings of molecules at the interface are responsible for the unique features of vibronic coupling.

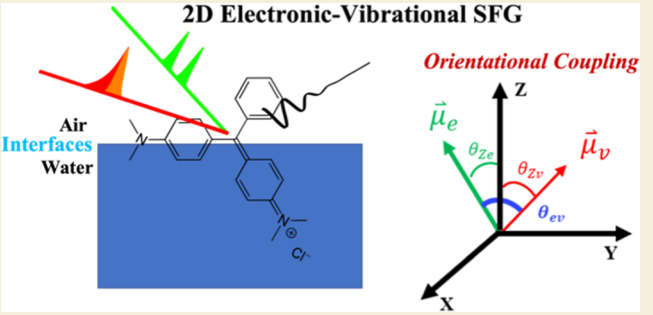

KEYWORDS: *vibronic coupling, orientational coupling, two-dimensional electronic−vibrational sum frequency generation, ultrafast interfacial processes, double-resonant sum frequency generation, intramolecular charge transfer*

INTRODUCTION

Vibronic couplings could occur when vibronic transitions are coupled with changes in the nuclear geometry.[1] For a pure electronic transition, vibronic couplings never happen since no nuclear motions are involved. The magnitude of mode-specific vibronic coupling reflects the degree of vibronic interactions of molecules at interfaces. The nucleic motions move on adiabatic potential energy surfaces under the Born−Oppenheimer approximation. The separated motions of nuclei and electrons are separated with negligible vibronic couplings within the approximation. Under the zeroth-order approximation, the amplitude of electronic transition is the product of transition strength and Franck−Condon factor of a vibrational wavefunction of the ground state and an excited vibrational wavefunction of a vibronic state. In this case, electronic transitions are independent of nuclear coordinates. On the other hand, the Born−Oppenheimer approximation is no longer valid, and vibronic couplings could become dominant when two adiabatic potential energy surfaces of excited states overlap. One shall turn to the Herzberg−Teller approximation, stating that electronic states depend on the nuclear coordinate.[1] In fact, the magnitude of vibronic couplings is so large that wave functions could transition from one adiabatic potential energy surface to another, leading to nonadiabatic phenomena such as nonradiative relaxation.

Photoinduced excited-state relaxation pathways of polyatomic molecules in bulk solids, solutions, and gases are of central importance in photochemistry and photophysics.[2−4] These relaxation processes of excited states are involved in

Received: February 15, 2023
Revised: April 6, 2023
Accepted: April 14, 2023
Published: May 5, 2023

https://doi.org/10.1021/jacsau.3c00074
JACS Au 2023, 3, 1413−1423

both electron and nuclear interactions, so-called vibronic couplings. Vibronic couplings are crucial to understanding nonadiabatic processes, especially near points of conical intersections.[1] These couplings are observed in photoinduced charge transfer, proton transfer, proton-coupled charge transfer, photoinduced isomerization, and energy transfer processes. Vibronic couplings play a key role in determining the rate constants for these reactions and physical processes. Recent studies have demonstrated that two-dimensional electronic−vibrational (2D-EV) and two-dimensional vibrational−electronic (2D-VE) spectroscopies can directly probe intermolecular or intramolecular vibronic couplings of molecules in bulk.[5−17] These spectroscopies have been applied to understand the correlation of electronic and vibrational dynamics during ultrafast photochemical reaction dynamics of molecules. On the other hand, photoinduced excited-state relaxation processes at interfaces play vital roles in many fields such as solar energy conversion, photocatalysis, and photosynthesis. Vibronic couplings at interfaces are expected to be different from those in bulk due to the unique environment. However, vibronic couplings at interfaces have not been well understood.

Although interface-specific doubly resonant sum frequency generation (DR-SFG) has been developed to study electronic−vibrational couplings of interfacial molecules,[18−34] this method is limited to electronic−vibrational couplings of the ground states of interfacial molecules. This DR-SFG technique measures both electronic transitions and vibrational transitions in the frequency domain, losing time-dependent structural evolution information. Recently, two-dimensional vibrational sum frequency generation spectroscopy (2D-VSFG)[35−41] and two-dimensional electronic sum frequency spectroscopy (2D-ESFG)[42,43] in the time domain have been developed to study vibrational coupling and electronic couplings as well as their structural dynamics at interfaces. Our preliminary efforts show that 2D electronic−vibrational sum frequency generation spectroscopy (2D-EVSFG) is a promising tool to reveal vibronic couplings in the structural evolution of excited states at interfaces[44] and may be extended to ultrafast time domains. Interfaces, distinct from bulk media, hold unique physical and chemical properties. Molecules are partially or fully orientationally ordered at interfaces. Unlike in a bulk solution, electronic dipoles and vibrational dipoles at interfaces cannot rotate freely due to the restricted interfacial environments. Thus, we anticipate that vibronic couplings at interfaces are different from those in bulk. The strength of vibronic couplings at interfaces depends critically on relative orientations of an electronic transition dipole and a vibrational transition dipole. However, we lack the knowledge of quantitative vibronic couplings of electronic and vibrational dipoles at interfaces. Our 2D-EVSFG experiments will help us address ultrafast interactions of electron and nuclear motions at interfaces. The goal of the 2D-EVSFG work is to fill the knowledge gap in quantifying vibronic couplings at interfaces.

In this work, we quantitatively determine orientational couplings in polarized 2D-EVSFG measurements to properly evaluate couplings of electronic and vibrational transition dipoles at interfaces. Furthermore, we demonstrate that molecules at interfaces exhibit different dynamic vibronic couplings from those in bulk.

EXPERIMENTAL SECTION

Laser System

A 1 kHz Ti/sapphire amplifier (UpTek Solution) (800 nm, 4 W, 100 fs) was used in 2D-EVSFG experiments. A small portion of 0.8 mJ from the amplifier was guided toward a home-built noncollinear optical parametric amplifier (NOPA) to generate the visible pump pulses, producing a 9.0 μJ output centered at 600 nm with a spectral width of 25 nm. This broad pulse was further compressed with a pair of prisms (LaK21, Newport) to be as short as 25−30 fs with a bandwidth less than 600 cm^{-1}. Thus, vibrational modes higher than 1200 cm^{-1} in the ground state were not excited due to the bandwidth of the pump pulse. The remaining portion of the amplifier was directed to an OPA (TOPAS, light conversion) to generate a broadband mid-IR with an output energy of 10 μJ. An etalon filter was used to obtain the narrow picosecond light from the dump beam out of the TOPAS.

2D-EVSFG Experiments

A translating wedge-based identical pulse encoding system (TWINS) was assembled to generate a pair of coherent pump pulses, by following the work of Cerullo and co-workers.[42,45,46] A detailed description of the TWINS and its calibration has been provided previously.[42,43] The time delay of the coherent pair, t_1, was incremented in 0.32 fs time steps from 0 to 80 fs. The time delay between the narrow picosecond and the broadband mid-IR was varied by a manual stage. A motorized translational stage served to adjust the delay, T_w, between the pump pair and the 800 nm/IR beams. A reflection geometry was used for 2D-EVSFG experiments. The pump pulses were inclined at 40° relative to the surface normal. The mid-IR and picosecond beams were combined by a dichroic mirror (ISP optics) for collinear propagation, followed by a 1″ CaF_2 lens (f = 75 mm) focused on samples at an angle of 60° relative to the surface normal. The polarization of the two pump beams, 2D-EVSFG, 800 nm, and IR beams were set to p-, p-, s-/p-, s-/p-, and p-polarized (PPSSP/PPPPP), respectively. To avoid the absorption of the IR beam by ambient humidity, a sealed box with a continuous purge of dry air was used to keep the relative humidity below 1%.

Electronic SHG (ESHG) and Time-Resolved ESHG (TR-ESHG) Experiments

A detailed description of the ESHG and TR-ESHG experiments has been provided previously.[22,43,47−50] Briefly, a broadband short-wave IR (SWIR) from 1150 to 2200 nm was generated by a home-built optical parametric amplifier. A short-pass filter cutoff at 1500 nm was used to keep the SWIR from 1150 to 1500 nm for ESHG experiments. To implement TR-ESHG experiments, a femtosecond laser of 600 nm was generated from the NOPA as a pump. We collected polarized interfacial electronic spectra of malachite green (MG) molecules by using the recently developed broadband electronic second harmonic generation (ESHG) technique.[43,48] Two polarization combinations of S-in/P-out and P-in/P-out were used in our measurements. "-in" denotes the polarization of an incident light, and "-out" denotes that of an output signal.

Detection System

A liquid nitrogen-cooled charge-coupled device (CCD) detector (Princeton Instrument, back-illuminated 1300 × 400) was integrated with a spectrometer (Andor-2300i, Princeton Instrument) for 2D-EVSFG signal detection. A Galvo mirror (Thorlabs) was synchronized with an optical chopper with half of the laser frequency, to spatially separate pump-on from pump-off signals onto the CCD. Two cylindrical lenses were positioned vertically (f = 25 cm) and horizontally (f = 10 cm) to provide both spatial and spectral resolution of the signals. A LabVIEW program was used to interface the stages and CCD with a computer. Each data point for 2D-EVSFG was integrated for 10 s and averaged 10 times.

Computational Details

To account for the solvation effect in the energy profiles of the ground (S_0) and first excited (S_1) states of the MG molecule, the following

https://doi.org/10.1021/jacsau.3c00074
JACS Au 2023, 3, 1413−1423

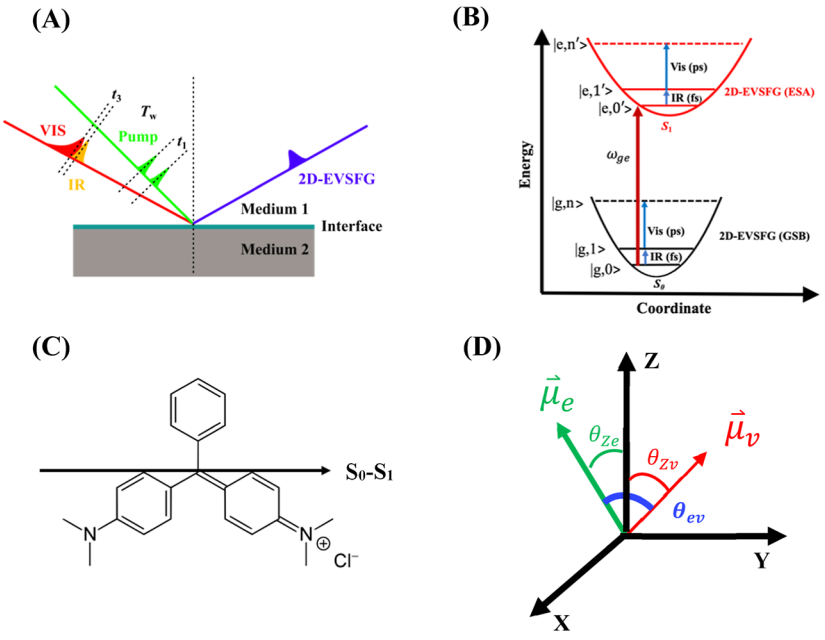

Figure 1. (A) Schematic setup of 2D-EVSFG spectroscopy and pulse sequences of the four involved lasers, including a pair of phase-locked pulses, a fs mid-IR, and a ps 800 nm. (B) Energy diagram for both ground state bleaching (GSB) and excited state absorption (ESA) in electronic−vibrational SFG pathways. (C) Chemical structure of MG and its transition dipole direction from S_0 to S_1. (D) Orientation of an electronic and a vibrational dipole with respect to the surface normal (Z).

equation was employed in our calculation: $E_{total} = E_{vac} + E_{sol}$, where a species' total energy, E_{total}, is the sum of its energy in vacuum, E_{vac}, and its solvation energy, E_{sol}. More specifically, E_{vac} was evaluated by the resolution-of-identity coupled cluster singles and doubles (RI-CC2) model[51] and the correlation consistent-polarized valence double zeta (cc-pVDZ) basis set,[52] while E_{sol} was computed by the molecular dynamics (MD) simulation in conjunction with the free energy perturbation method[53]

$$E_{sol} = \frac{1}{k_B T} \ln \langle e^{\Delta V / k_B T} \rangle \quad (1)$$

where k_B is the Boltzmann constant, $\langle\ \rangle$ denotes the average over the canonical ensemble at temperature T, and ΔV is the solute−solvent coupling energy. For each of the three conformations of MG at both S_0 and S_1 states, its atomic partial charges in the MD simulation were ascertained by the restrained electrostatic potential (RESP) approach,[54] while its bonded and nonbonded force field parameters were adopted from the general AMBER force field (GAFF).[55] In our MD simulation, the MG molecule was solvated by 1023 water molecules as a 42 Å × 42 Å slab to mimic the air/water interface. Along the normal of the slab, our simulation box was 40 Å long to diminish artifacts caused by interactions between system images under the periodic boundary condition. All water molecules were represented by the flexible simple point-charge (SPC/Fw) water model.[56] Unless otherwise specified, all RI-CC2 simulations were carried out by the TURBOMOLE package,[57] and all MD calculations were conducted by the CP2K software.[58]

Chemicals

MG from Acros Organics was used as received. Ultrapure water of 18 MΩ·cm was used to prepare samples in all experiments.

RESULTS

2D-EVSFG experiments consisted of four laser pulses, including two phase-locked femtosecond (fs) visibly resonant pulses (E_{p1} and E_{p2}), a fs mid-IR resonant pulse (E_{IR}), and a ps 800 nm pulse (E_{ps}), as shown in Figure 1A. The 2D-EVSFG signal coherently radiates in a direction obeying both energy and momentum conservations. The purely adsorptive 2D-EVSFG is achieved in a pump−probe geometry.[59] The temporal delays of the four pulses are defined as the time gap between the pulse maxima of their envelopes, specified as t_1, T_w, t_3, and t, respectively (we used T_w to replace t_2 here).[44] The time delay, t_1, is scanned for each waiting time of T_w, while the time delay of t is measured in the frequency domain and the time delay of t_3 is fixed. 2D-EVSFG spectra contain both negative ground state bleaching (GSB) and positive excited state absorption (ESA), as schematically shown in Figure 1B. The phase-locked fs pulses excite vibronic transitions from a vibronic state, $|g,v\rangle$, in the ground state, S_0, to a vibronic state, $|e,v'\rangle$, in the first excited state, S_1. Thus, we probe both GSB and ESA fourth-order polarizations, $P^{(4)}(\omega_1, T_w, \omega_t; t_3)$. The 2D-EVSFG electric field is a product of three parts, including transition amplitude function in ( ), orientational function in $\langle\rangle_{T_w}$, and line-shape function, $F(\omega_1, T_w, \omega_t; t_3)$, which takes the form

$$E^{(4)}(\omega_1, T_w, \omega_t; t_3) \propto (\alpha \mu_V \mu_{gv,ev'} \mu_{gv,ev'}) \langle Y_{aa'} Y_{bb'} Y_{cc'} Y_{dd'} Y_{ee'} \rangle_{T_w} F(\omega_1, T_w, \omega_t; t_3) \quad (2)$$

where ω_t is the energy of sum frequency, $\omega_{SFG} = \omega_{vis} + \omega_{IR}$, $\mu_{gv,ev'}$ is the amplitude of an electronic dipole moments for the visibly resonant pulses (1 and 2), μ_V is the amplitude of a vibrational dipole moment, and α is the vibrational polarizability amplitude. $Y_{aa'}$ denotes the spherical harmonic form of the orientational function as adopted in a standard form.[60] Here, we focus on the transition amplitude function and the orientational function. The line shape of the 2D-EVSFG peaks will be reported separately. From eq 2, it is seen that the intensity of 2D-EVSFG is related to both the transition amplitude and the relative orientation of electronic transition dipoles and vibrational dipoles of interest. The directions of the electronic transition dipole from S_0 to S_1 for MG and its

https://doi.org/10.1021/jacsau.3c00074
JACS Au 2023, 3, 1413−1423

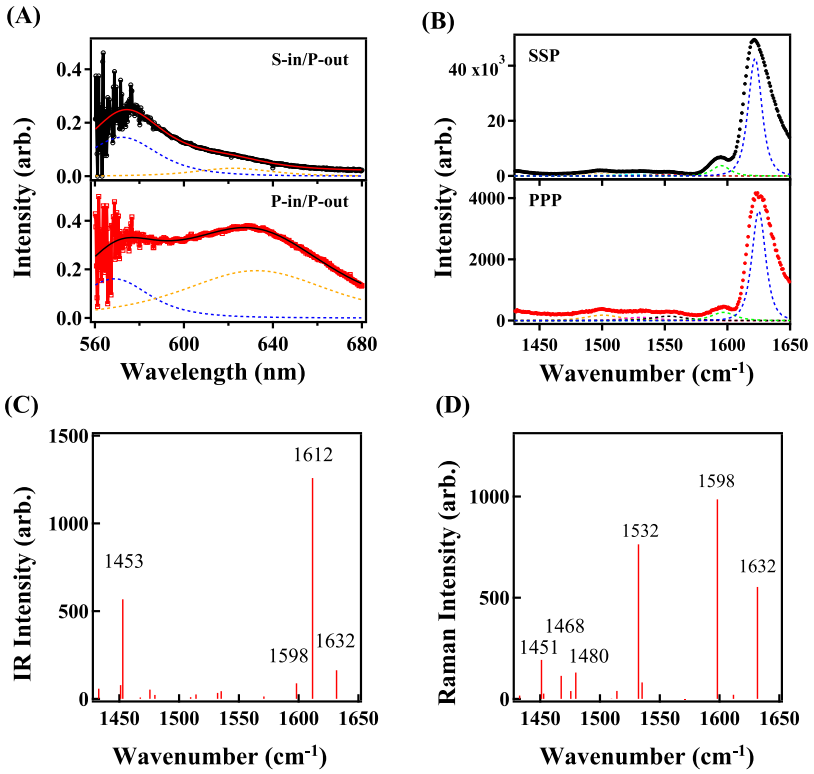

Figure 2. (A) ESHG spectra of 150 μM MG at the air/water interface under S-in/P-out (top) and P-in/P-out (bottom) polarization combinations. (B) VSFG spectra of 150 μM MG at the air/water interface under SSP (top) and PPP (bottom) polarization combinations. Calculated IR (C) and Raman (D) spectra in the ground state of MG.

chemical structure are presented in Figure 1C. The electronic transition dipole from S_0 to S_1 is along the molecular long axis of MG, which is perpendicular to the vertical molecular symmetry axis.[61] The orientation of electronic and vibrational dipoles with respect to the surface normal and their relative orientation are schematically depicted in Figure 1D. Thus, 2D-EVSFG probes the correlation of an electronic dipole and different vibrational dipoles.

To assign peaks and quantify orientational couplings in 2D-EVSFG spectra, we shall examine one-dimensional electronic and vibrational spectra of MG at the air/water interface. Broadband ESHG spectra of 150 μM MG from the air/water interface were taken, as shown in Figure 2A. Fitting of the spectra yielded two peaks at 633.0 and 568.0 nm in the P-in/P-out ESHG spectrum, while one dominant peak at 568.0 nm in the S-in/P-out spectrum was observed. From the polarized ESHG data, an orientational angle of the electronic transition dipole for S_0−S_1 was found to be ca. 37° with respect to the surface normal. Figure 2B shows VSFG spectra of 150 μM MG at the air/water interface for both SSP and PPP polarization combinations. Three main peaks are located at 1622.0, 1594.0, and 1499.6 cm^{-1}. The calculated IR and Raman spectra are also shown in Figure 2C,D, respectively. Only the calculated peaks at 1632.0 and 1598 cm^{-1} are both Raman and IR active, corresponding to the peaks at 1622.0 and 1594.0 cm^{-1} in VSFG spectra, respectively. The calculated peak at 1532.0 cm^{-1} is only Raman active and is weak due to the forbidden IR activity, corresponding to the peak at 1499.6 cm^{-1} in the VSFG spectra. Thus, the peaks at 1622.0, 1594.0, and 1499.6 cm^{-1} are attributed to −C═C− stretching, in-plane ring stretching and bending, and NR_2 bending and rocking modes, respectively.[62] These vibrations are also visualized in Figure S1. In addition, the calculated SFG intensities of MG in the ground state are shown in Figure S2.

Polarized 2D-EVSFG Measurements

Figure 3A,B presents 2D-EVSFG spectra of 150 μM MG molecules at the air/water interface at a waiting time T_w of 0 fs under polarization combinations of both PPSSP (A) and PPPPP (B). It appears that the two polarized 2D spectra share common spectral features along both the electronic and vibrational axes. The main differences in the two polarized spectra are as follows: (1) the peak amplitudes in the two polarized spectra are significantly different; (2) the peak at 1594.0 cm^{-1} is negative in the PPSSP but positive in the PPPPP, which is due likely due to the spectral overlap of a negative GSB peak at 1592.0 cm^{-1} with a positive and spectrally shifted ESA peak of the 1622.0 cm^{-1} mode.

Figure 3C,D displays sliced electronic excitation spectra at selected representative vibrations of 1622.0, 1567.0, 1520.0, and 1464.0 cm^{-1} under PPSSP and those of 1626.0, 1576.0, 1520.0, and 1466.0 cm^{-1} under PPPPP. There are four accessible vibronic transition (VT) peaks at 583.6, 602.1, 614.8, and 628.5 nm under PPSSP and only the latter three under PPPPP for both the positive ESA peaks and the negative GSB. The vibronic absorption peaks for MG molecules at the interface in 2D-EVSFG are prominent, which are distinct from those in bulk in 2D-EV spectra.[17] These unique features at the interface might be attributed to the fact that there are different selection rules for interface-specific spectra than the bulk. These results imply that 2D-EVSFG probes unique interfacial properties of molecules. The 2D-EVSFG line shapes are determined by a vibrational linewidth, Γ_{ν}, and an electronic linewidth, Γ_{eg}, along the vibrational and electronic axes, respectively. It was found that more VT peaks are seen in

https://doi.org/10.1021/jacsau.3c00074
JACS Au 2023, 3, 1413−1423

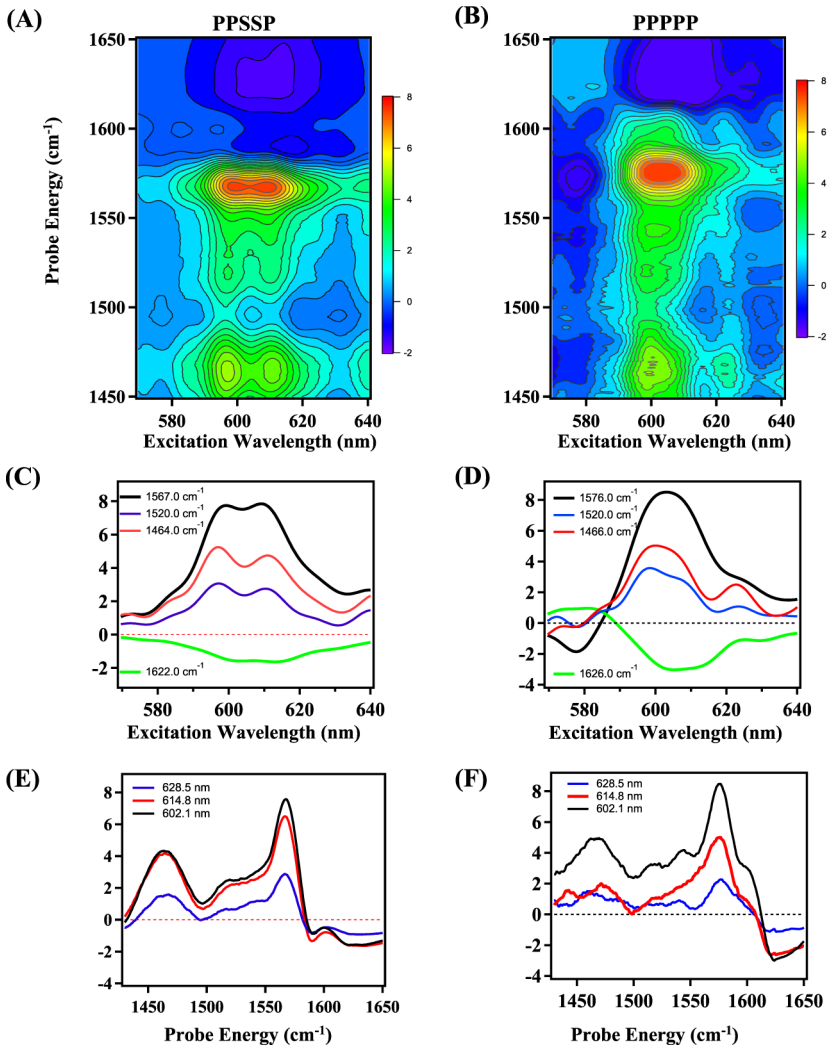

Figure 3. 2D-EVSFG spectra of 150 μM MG molecules at the air/water interface for PPSSP (A) and PPPPP (B) at a waiting time of 0 fs. Sliced electronic spectra (C) and vibrational spectra (E) from (A). Sliced electronic spectra (D) and vibrational spectra (F) from (B). Negative: GSB. Positive: ESA.

2D-EVSFG than those in steady-state ESHG in Figure 2A. The ESA VT transitions are blue-shifted with respect to their GSB counterparts, originating from the anharmonicity of the vibronic potential energy surfaces for different vibronic states as we observed previously.[44,63] Spectral shifts between ESA and GSB in two-dimensional electronic−vibrational spectra were found to be possible when quadratic vibronic coupling became significant for mode mixing.[17]

Figure 3E,F shows sliced vibrational spectra at the three main VT peaks of 628.5, 614.8, and 602.1 nm. Two negative GSB peaks occur at ω_t = 1594.0 and 1622.0 cm^{-1} for PPSSP and only one negative peak at 1626.0 cm^{-1} for PPPPP. These two negative peaks correspond to those in steady-state VSFG in Figure 2B. Such a difference in the GSB peaks suggests that the two vibrational dipoles exhibit different orientations with respect to the electronic dipole of MG at the interface. As seen in Figure 3E,F, two positive ESA peaks are observed at 1576.0 and 1464.0 cm^{-1} in both the spectra, which were assigned to those spectrally shifted in the excited state with respect to the peaks at 1594.0 and 1499.6 cm^{-1} in the ground state, respectively. The calculated SFG intensities of MG in the S_1 excited state are shown in Figure S3. In addition, the positive peak shows up at 1594.0 cm^{-1} in PPSSP, which is due to the anharmonic shift to the red from 1622.0 cm^{-1} in the ground state. The resultant spectral shifts are found to be 28.0, 35.6, and 28.0 cm^{-1}, respectively. Such significant shifts in vibrational spectra suggest that the locally excited state of MG possesses more diffusive curvatures of the potential energy surface than those in its ground state.

Strength of Vibronic Coupling

The strength of vibronic coupling is related to the electronic transition dipole moment coupled with vibrations over the ground and excited states of molecules.[16,63] According to the Franck−Condon and Born−Oppenheimer approximations, the amplitudes of 2D-EVSFG are simply proportional to the square of the product of the electronic transition amplitude and Franck−Condon factors, namely, $|\mu_{eg}^{(0)}|^2|\langle g, \nu|e, \nu'\rangle|^2$. In this case, electronic transitions are independent of nuclear coordinates, and no vibronic couplings occur. On the other hand, the Condon approximation is broken when electronic transitions are involved in nuclear geometries. Such a nuclear-dependent transition results in vibronic couplings. To reveal if vibronic couplings take place upon photoexcitation at interfaces, we further analyzed three transitions of 625.2, 609.7, and 596.5 nm for the ESA peak of 1567.0 cm^{-1}. The

https://doi.org/10.1021/jacsau.3c00074
JACS Au 2023, 3, 1413−1423

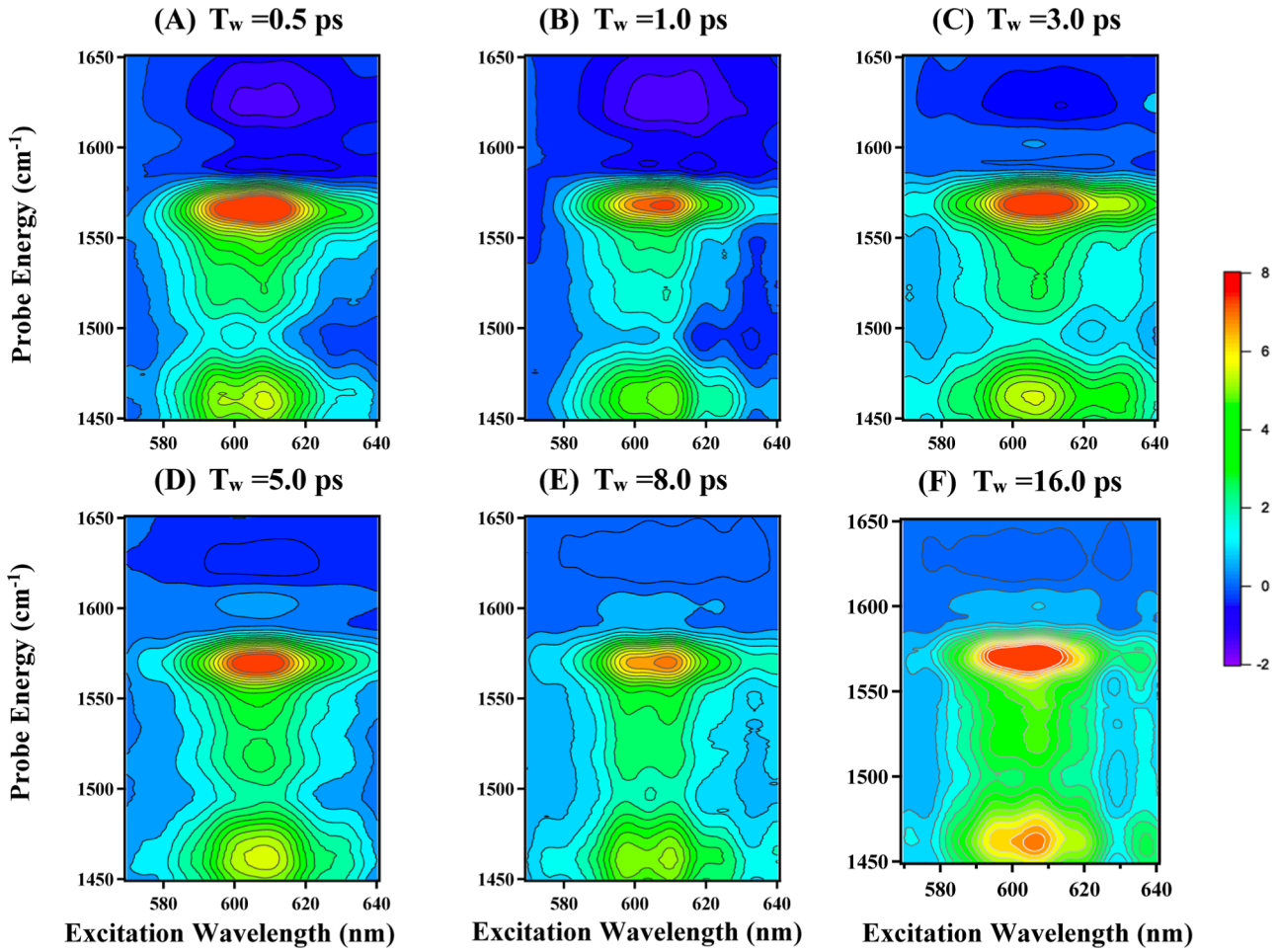

Figure 4. Time-dependent PPSSP polarized 2D-EVSFG spectra of MG at the air/water interface at different waiting times of 0.5 (A), 1.0 (B), 3.0 (C), 5.0 (D), 8.0 (E), and 16.0 ps (F). (A) T_w = 16.0 ps, (B) T_w = 8.0 ps, (C) T_w = 5.0 ps, (D) T_w = 3.0 ps, (E) T_w = 1.0 ps, and (F) T_w = 0.5 ps.

lowest transition at 625.2 nm is considered to be $|g,0\rangle$ to $|e,0'\rangle$. Thus, the other two peaks at 609.7 and 596.5 nm correspond to vibronic transitions with low-frequency vibrations of 406.6 and 798.0 cm^{-1} from $|g,0\rangle$ to $|e,1'\rangle$ and $|e,2'\rangle$. The latter was approximated to be an overtone of the former. According to eq 2, the intensity ratio for the three VT peaks is equal to $|\mu_{g0,e2'}|^2:|\mu_{g0,e1'}|^2:|\mu_{g0,e0'}|^2$ for the same vibrational mode of 1567.0 cm^{-1}. Within the zeroth-order approximation, such a ratio is related to their Franck−Condon factors, namely, $\langle g,0|e,2'\rangle^2:\langle g,0|e,1'\rangle^2:1$. If the photoexcitation results only in a displaced excited state, the Huang−Rhys coefficient, S, could be evaluated. The value of S is estimated to be as high as 2.25 for this mode. On the other hand, our computations show that the Franck−Condon factor at 461.8 cm^{-1} close to the experimentally measured 406.6 cm^{-1} has a value of 0.146, as displayed in Table S1. Such a large difference in S suggests that nuclear-dependent Herzberg−Teller vibronic couplings might play an important role in the photoexcitation.

Orientational Correlations of an Electronic Transition Dipole and a Vibrational Transition Dipole

Vibronic transitions are involved in pure electronic transitions, namely, from $|g0\rangle$ to $|e0\rangle$. As shown in Figure 3, the lowest transition of MG occurs at 628.5 nm, which is considered to be a pure electronic transition. In other words, no vibronic coupling in this case occurs. Thus, we shall employ the vibrational peaks for the electronic transition at 628.5 nm to analyze orientational information. To obtain the relative angle, θ_{ev}, of the electronic transition dipole and the vibrational dipole, we consider only the orientational function upon photoexcitation, namely, T_w = 0. The time evolution of the orientational function will be described in a separate document. To be concise, we use $\langle\ \rangle$ at T_w = 0 hereafter. Here, an orientational angle of electronic transition dipole, θ_{Ze}, is expressed by a vibrational dipole, θ_{Zv}, as defined in Figure 1C. In the case of the polarization combination of *ZZZZZ*, a fourth-order orientational response function in the laboratory coordinate system, (X, Y, Z), takes the form of

$$\begin{aligned}\langle Y_{Ze}Y_{Ze}Y_{Zv}Y_{Zv}Y_{Zv}\rangle &= \left\langle \frac{3}{2}\cos^3\theta_{Ze}\sin^2\theta_{ev}\cos\theta_{ev} \right. \\ &\quad \left. - \cos^5\theta_{Ze}\left(\frac{3}{2}\cos\theta_{ev} + \frac{5}{2}\cos^3\theta_{ev}\right)\right\rangle \\ &= \left(\left\langle \frac{3}{2}\sin^2\theta_{ev}\cos\theta_{ev}\right\rangle \right. \\ &\quad \left. - D'_{3S}\left\langle\left(\frac{3}{2}\cos\theta_{ev} - \frac{5}{2}\cos^3\theta_{ev}\right)\right\rangle\right) \\ &\quad \langle\cos^3\theta_{Ze}\rangle \end{aligned} \quad (3)$$

https://doi.org/10.1021/jacsau.3c00074
JACS Au 2023, 3, 1413−1423

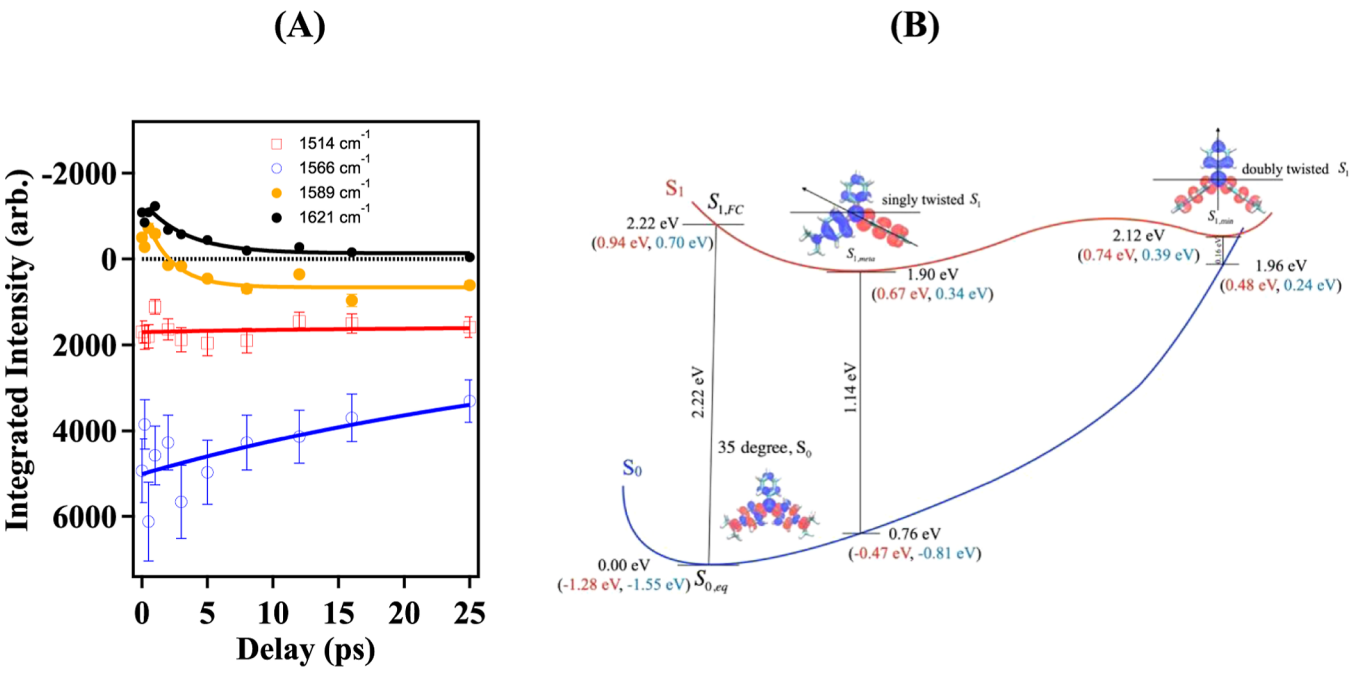

Figure 5. (A) Time-dependent 2D-EVSFG intensities at 1514, 1566, 1589, and 1621 cm^{-1}. (B) Simulated schematic PESs of MG at the air/water interface (black), in the bulk (blue), and in vacuum (red), respectively.

In the case of the polarization combination of *ZZYYZ*, *ZZXXZ*, and *ZZXZX*, a fourth-order orientational response function in the laboratory coordinate system takes the form of

$$\begin{aligned}&\langle Y_{Ze}Y_{Ze}Y_{Yv}Y_{Yv}Y_{Zv}\rangle = \langle Y_{Ze}Y_{Ze}Y_{Xv}Y_{Xv}Y_{Zv}\rangle = \langle Y_{Ze}Y_{Ze}Y_{Xv}Y_{Zv}Y_{Xv}\rangle \\ &= \langle Y_{Ze}Y_{Ze}Y_{Zv}Y_{Xv}Y_{Xv}\rangle = \frac{1}{2} \\ &\left\langle \cos^3\theta_{Ze}\left(\cos\theta_{ev} - \frac{3}{2}\sin^2\theta_{ev}\cos\theta_{ev}\right)\right. \\ &\left. + \cos^5\theta_{Ze}\left(\frac{3}{2}\sin^2\theta_{ev}\cos\theta_{ev} - \cos^3\theta_{ev}\right)\right\rangle \\ &= \frac{1}{2}\left(\left\langle\left(\cos\theta_{ev} - \frac{3}{2}\sin^2\theta_{ev}\cos\theta_{ev}\right)\right\rangle \right. \\ &\left. + D_{35}'\left\langle\left(\frac{3}{2}\sin^2\theta_{ev}\cos\theta_{ev} - \cos^3\theta_{ev}\right)\right\rangle\right)\langle\cos^3\theta_{Ze}\rangle \end{aligned} \quad (4)$$

where

$$D_{35}' = \frac{1}{D_{35}} = \frac{\langle\cos^5\theta_{Ze}\rangle}{\langle\cos^3\theta_{Ze}\rangle} \quad (5)$$

Equation 4 is directly related to the intensity of PPSSP by nonlinear Fresnel coefficients and incident angles, while a combination of eq 3 with eq 4 contributes to the intensity of PPPPP.

To extract the orientational order parameter, D_{35}, we turn to time-dependent visible-pump polarized ESHG experiments.[64,65] Time-dependent ESHG kinetic traces for S-in/P-out and P-in/P-out under a fs pump of 600 nm are shown in Figure S4. From the kinetic data at $t = 0$, we obtained the value of 1.546 for D_{35}. Furthermore, we retrieved the relative orientation angle, θ_{ev}, of an electronic transition dipole and a vibrational transition dipole by combining eqs 4 and 5 with experimentally measured intensities of vibrational peaks of interest under PPSSP and PPPPP. A detailed derivation of the fourth-order orientational response functions for 2D-EVSFG is found in the Supporting Information. Based on eqs 3−5, the intensity ratio of PPPPP and PPSSP was plotted as a function of θ_{ev} in Figure S5. We chose two vibrational modes of 1622.0 and 1499.6 cm^{-1} in the ground state to compare their relative orientations with respect to the electronic transition dipole. It was found that the two vibrational dipoles are oriented with respect to the electronic transition dipole from S_0 to at 31.5 ± 3.0° and 35.5 ± 3.5°. These results are consistent with those from our calculations as shown in Figure S6.

Time-Dependent 2D-EVSFG Measurements

To reveal the time evolution of the excited state of interfacial MG molecules, 2D-EVSFG spectra were collected at different waiting times. Figure 4 presents four representative 2D-EVSFG spectra under PPSSP for six waiting times of 0.5 (A), 1.0 (B), 3.0 (C), 5.0 (D), 8.0 (E), and 16.0 ps (F). From the early time to the late time, the two GSB peaks at 1594.0 and 1622.0 cm^{-1} and the three ESA peaks at 1520.0 and 1566.0 cm^{-1} become weaker. An additional peak at 1598.0 cm^{-1} shows up after T_w = 3.0 ps. As the T_w increases, the signal for the peak gets stronger. Furthermore, the spectral width at 1566.0 cm^{-1} becomes narrower as the waiting time increases, suggesting that the diffusive locally excited state evolves into an intramolecular charge transfer state. As compared with those in bulk,[17] the structural evolution at the interface is significantly different.

Structural Evolution of Photoinduced Excited States

To examine the structural evolution of MG molecules at the air/water interface, we chose to track time-dependent changes in 2D-ESFG spectra. We integrated the area for three vibrational peaks at 1590.0 ± 5.0, 1566.0 ± 5.0, and 1514 ± 5.0 cm^{-1} from 600 to 620 nm. Figure 5A shows kinetic behaviors of the three peaks. The GSB peak at 1621.0 cm^{-1} exhibits a fast recovery time of 3.3 ± 0.3 ps and a very long recovery process. Such a process is much faster than that of 8.1

https://doi.org/10.1021/jacsau.3c00074
JACS Au 2023, 3, 1413−1423

± 0.3 ps in bulk methanol.[17] The ESA peak of 1566.0 cm^{-1}, generated instantaneously upon photoexcitation, relaxes as slowly as 38.5 ± 2.0 ps, while the corresponding peak in bulk has two relaxation time constants of 4.7 ± 1.7 ps and 9.0 ± 3.5 ps.[17] Although the time traces for the ESA peak of 1566.0 cm^{-1} were not satisfactory, our results may give some qualitative guidance on how the interfacial relaxations are different than those in the bulk. Additionally, the newly generated ESA peak at 1590.0 cm^{-1} shows only a fast rise time constant of 2.1 ± 0.3 ps at the air/water interface and a much longer decay time constant. On the other hand, its corresponding peak in methanol exhibits a similar rise time constant of 1.5 ± 0.2 ps but decays with a time constant of 7.9 ± 0.8 ps.[17]

Figure 5B shows that our calculated energy gap between the singly twisted S_1 and the doubly twisted S_1 drastically drops from 0.22 to 0.07 eV upon being solvated at the air/water interface, greatly facilitating the conformational change from the locally excited S_1 to the doubly twisted S_1 that otherwise would be energetically prohibitive in a vacuum. This change can be partially ascribed to the solvation energy penalty on the more polarized singly twisted S_1 at the asymmetric air/water interface if one considers its dipole moment of 9.70 Debye compared to 7.47 Debye of the doubly twisted S_1. Moreover, our calculated IR intensity of the 1598 cm^{-1} mode of the doubly twisted S_1 is 275.6 km/mol, which is ∼1000 times greater than that of its S_0 counterpart of 0.32 km/mol at 1589 cm^{-1}. This greatly enhanced IR intensity upon excitation suggests that our 2D-EVSFG signal near 1590 cm^{-1} arises from the excited state, instead of the ground state.

The change of 2D-EVSFG peak intensity is a convolution of the changes in the vibrational oscillator strength and population, as described in the 2D-EV experiments.[17] It is challenging to assign the peaks at the excited state of MG. In bulk, the peak at 1566.0 cm^{-1} was attributed to one of two minima of the first excited state, $S_{1,min}$, while the peak 1590.0 cm^{-1} was due to the twisted ground state geometry. From the kinetic data, we attempted to assign the peaks to the excited state geometries of MG at the air/water interface. The peak at 1566 cm^{-1}, which increases with instantaneous generation, was assigned to be the excited state geometry closest to the Franck−Condon geometry. Previous ab initio calculations showed that vibrational oscillator strength increases as molecules relax from the locally excited Franck−Condon geometry to the singly twisted excited state.[17] However, the peak at 1589 cm^{-1} could not be the twisted ground state geometry in our case, unlike that in bulk methanol.[17] The peak 1590.0 cm^{-1} in the 2D-EVSFG spectra did not decay to zero even after 20 ps, which is longer than that of a twisted ground state. Thus, the peak at 1589 cm^{-1} was assigned to be the doubly twisted excited state at the interface.

Previous 2D-EV studies of MG in bulk demonstrated that the photoinduced relaxation of MG experiences both intramolecular charge transfer and conical intersection dynamics.[17] Time-resolved second harmonic generation experiments showed that the excited state of MG is viscosity dependent.[66] To reveal the structural evolution of MG, we implemented MD simulations to calculate the minimum energy structures of the ground and excited potential energy surfaces (PES) of MG at the air/water interface. Figure 5B shows a schematic PES for MG at the air/water interface. The gap energy of S_0 and the locally excited S_1 was found to be ca. 2.22 eV. For the excited state S_1, there are two geometric minima; one is singly twisted, and the other is doubly twisted. Their energies are 0.27 and 0.20 eV lower than those of the locally excited S_1. There are two structural differences between the air/water interface and bulk methanol. The first one is that only one minimum, $S_{1,min}$, exists at the air/water interface. The minima $S_{1,min'}$ in bulk were not found in our calculations, suggesting that the $S_{1,min'}$ structure is not stable in the hydrophobic nature of the interface. The other one is the drastically reduced energy gap between the singly and doubly twisted excited states. Furthermore, the energy level of the doubly twisted excited state geometry is 0.16 eV higher than that of the singly twisted ground state. The solvation effect does lower the energy gap between the singly and doubly twisted states to ∼0.07 eV, making them essentially degenerate in energy. Thus, it was suggested that the air/water interface favors the formation of the doubly twisted excited state of MG. The photoexcited state relaxes from the Franck−Condon region at a time scale of 2.1 ± 0.3 ps. Due to the restricted environment, MG molecules could not rotate freely with the twisted excited state and take long to relax to the ground state. Unlike in bulk methanol, conical interactions do not occur within our observed time window. The unique restricted environment does not favor the twisted excited state to relax fast enough to be coupled with a twisted ground state through a conical interaction. The orientational orderings of molecules at the interface block the excited state from rotating freely for the unique features of vibronic couplings.

CONCLUSIONS

We have examined orientational correlations and vibronic couplings of electronic and vibrational transition dipoles as well as the structural evolution of photoinduced excited states of MG molecules at the air/water interface by developing a two-dimensional electronic−vibrational sum frequency generation (2D-EVSFG). Our main findings from 2D-EVSFG spectra revealed unique orientation correlations in electronic−vibrational couplings of molecules at the air/water interface. The novelty of this work is that we have not only quantified orientational couplings of an electronic dipole and a vibrational dipole upon photoexcitation at interfaces but also shown that dynamical vibronic couplings at interfaces are different from those in bulk. Structural evolution of photoinduced excited states exhibits distinct behaviors at the interface. Specifically, we have made the following discoveries:

- Vibronic absorption peaks in 2D-EVSFG for MG molecules at the interface are more prominent than those in bulk in 2D-EV spectra.
- Together with polarized VSFG and ESHG experiments, polarized 2D-EVSFG spectra were used to extract relative orientations of an electronic transition dipole and vibrational transition dipoles at the interface.
- Our quantitative analyses have shown that the vibronic transition of low-frequency vibrations of 406.6 cm^{-1} could not be explained by the Franck−Condon approximation. Rather, nuclear-dependent Herzberg−Teller vibronic couplings likely participate in the photoexcitation.
- Combined with MD calculations, time-dependent 2D-EVSFG experiments have demonstrated that the structural evolution of photoinduced excited states at the interface fails to exhibit significant conical interactions within 25 ps. Instead, the twisted excited state shows a long lifetime. Restricted environment and

https://doi.org/10.1021/jacsau.3c00074
JACS Au 2023, 3, 1413−1423

orientational orderings of molecules at the interface are likely responsible for the unique features of vibronic couplings.

In summary, we have demonstrated that 2D-EVSFG is a powerful tool to reveal properties of photoinduced excited states at interfaces. Dynamic vibronic coupling is intimately related to photoinduced relaxation processes at interfaces, such as solar energy conversion, photocatalysis, photoelectrocatalysis, artificial photosynthesis, and surface photochemistry for environmental chemistry, etc. Although the central objective of this work was to develop a conceptual framework for describing the dynamic vibronic couplings at interfaces, we believe that this new concept could be readily transformed to other interfacial systems that are relevant to the broader range of chemists in the field of material science, photochemistry, biophysics, and environmental chemistry as well as interface chemistry, theoretical chemistry, and spectroscopy.

■ ASSOCIATED CONTENT

Supporting Information

The Supporting Information is available free of charge at https://pubs.acs.org/doi/10.1021/jacsau.3c00074.

Visualization of vibrational modes from 1500 to 1650 cm^{-1} of MG; calculated SFG intensities of MG in the ground state; calculated SFG intensities of MG in the S_1 excited state; calculated Franck−Condon factor and Hyang−Rhys factor of MG molecules; time-dependent ESHG kinetic traces for S-in/P-out and P-in/P-out under a fs pump of 590 nm; intensity ratio of PPPPP to PPSSP as a function of the relative orientational angle; derivation of the fourth-order orientational response functions for 2D-EVSFG; and calculated relative orientational angles for vibrational modes of MG (PDF)

■ AUTHOR INFORMATION

Corresponding Author

Yi Rao − *Department of Chemistry and Biochemistry, Utah State University, Logan, Utah 84322, United States;* orcid.org/0000-0001-9882-1314; Email: yi.rao@usu.edu

Authors

Zhi-Chao Huang-Fu − *Department of Chemistry and Biochemistry, Utah State University, Logan, Utah 84322, United States*

Yuqin Qian − *Department of Chemistry and Biochemistry, Utah State University, Logan, Utah 84322, United States*

Tong Zhang − *Department of Chemistry and Biochemistry, Utah State University, Logan, Utah 84322, United States*

Gang-Hua Deng − *Department of Chemistry and Biochemistry, Utah State University, Logan, Utah 84322, United States*

Jesse B. Brown − *Department of Chemistry and Biochemistry, Utah State University, Logan, Utah 84322, United States*

Haley Fisher − *Department of Chemistry and Biochemistry, Utah State University, Logan, Utah 84322, United States*

Sydney Schmidt − *Department of Chemistry and Biochemistry, Utah State University, Logan, Utah 84322, United States*

Hanning Chen − *Texas Advanced Computing Center, The University of Texas at Austin, Austin, Texas 78758, United States;* orcid.org/0000-0003-3568-8039

Complete contact information is available at: https://pubs.acs.org/10.1021/jacsau.3c00074

Author Contributions

[§]Z.-C.H.-F. and Y.Q. contributed equally to this work. The manuscript was written through contributions of all authors. All authors have given approval to the final version of the manuscript. Z.-C.H.-F. and Y.Q.: conceptualization, investigation, methodology, writing—original draft; T.Z. and G.-H.D.: conceptualization, investigation, methodology; J.B.B. and S.S.: writing—review & editing; H.C.: funding acquisition, computation, writing—review and editing; Y.R.: funding acquisition, supervision, investigation, writing—review & editing.

Notes

The authors declare no competing financial interest.

■ ACKNOWLEDGMENTS

This material is based upon work supported by the National Science Foundation under grant no. [2045084]. Computational resources were provided by the Argonne Leadership Computing Facilities at the Argonne National Laboratory under the Department of Energy contract DE-AC-06CH11357 and by the Extreme Science and Engineering Discovery Environment at the Texas Advanced Computing Center under the National Science Foundation contract TG-CHE130008.

■ REFERENCES

(1) Fischer, G. *Vibronic Coupling: The Interaction between the Electronic and Nuclear Motions*; Academic Press, 1984; p 222.

(2) Turro, N. J.; Ramamurthy, V.; Scaiano, J. *Modern Molecular Photochemistry of Organic Molecules*; University Science Books, 2010; p 1053.

(3) Birks, J. B. *Organic Molecular Photophysics*; J. Wiley, 1975; p 653.

(4) Birks, J. B. *Organic Molecular Photophysics*; J. Wiley, 1973; p 600.

(5) Arsenault, E. A.; Schile, A. J.; Limmer, D. T.; Fleming, G. R. Vibronic Coupling in Energy Transfer Dynamics and Two-Dimensional Electronic-Vibrational Spectra. *J. Chem. Phys.* **2021**, *155*, 054201.

(6) Lewis, N. H.; Dong, H.; Oliver, T. A.; Fleming, G. R. A Method for the Direct Measurement of Electronic Site Populations in a Molecular Aggregate Using Two-Dimensional Electronic-Vibrational Spectroscopy. *J. Chem. Phys.* **2015**, *143*, 124203.

(7) Gaynor, J. D.; Courtney, T. L.; Balasubramanian, M.; Khalil, M. Fourier Transform Two-Dimensional Electronic-Vibrational Spectroscopy Using an Octave-Spanning Mid-Ir Probe. *Opt. Lett.* **2016**, *41*, 2895−2898.

(8) Lewis, N. H. C.; Gruenke, N. L.; Oliver, T. A. A.; Ballottari, M.; Bassi, R.; Fleming, G. R. Observation of Electronic Excitation Transfer through Light Harvesting Complex Ii Using Two-Dimensional Electronic-Vibrational Spectroscopy. *J. Phys. Chem. Lett.* **2016**, *7*, 4197−4206.

(9) Arsenault, E. A.; Bhattacharyya, P.; Yoneda, Y.; Fleming, G. R. Two-Dimensional Electronic-Vibrational Spectroscopy: Exploring the Interplay of Electrons and Nuclei in Excited State Molecular Dynamics. *J. Chem. Phys.* **2021**, *155*, 020901.

(10) Oliver, T. A.; Fleming, G. R. Following Coupled Electronic-Nuclear Motion through Conical Intersections in the Ultrafast Relaxation of Beta-Apo-8'-Carotenal. *J. Phys. Chem. B* **2015**, *119*, 11428−11441.

(11) Oliver, T. A.; Lewis, N. H.; Fleming, G. R. Correlating the Motion of Electrons and Nuclei with Two-Dimensional Electronic-Vibrational Spectroscopy. *Proc. Natl. Acad. Sci. U. S. A.* **2014**, *111*, 10061−10066.
(12) Yoneda, Y.; Arsenault, E. A.; Yang, S. J.; Orcutt, K.; Iwai, M.; Fleming, G. R. The Initial Charge Separation Step in Oxygenic Photosynthesis. *Nat. Commun.* **2022**, *13*, 2275.
(13) Courtney, T. L.; Fox, Z. W.; Slenkamp, K. M.; Khalil, M. Two-Dimensional Vibrational-Electronic Spectroscopy. *J. Chem. Phys.* **2015**, *143*, 154201.
(14) Gaynor, J. D.; Sandwisch, J.; Khalil, M. Vibronic Coherence Evolution in Multidimensional Ultrafast Photochemical Processes. *Nat. Commun.* **2019**, *10*, 5621.
(15) Lewis, N. H.; Fleming, G. R. Two-Dimensional Electronic-Vibrational Spectroscopy of Chlorophyll a and B. *J. Phys. Chem. Lett.* **2016**, *7*, 831−837.
(16) Fox, Z. W.; Blair, T. J.; Khalil, M. Determining the Orientation and Vibronic Couplings between Electronic and Vibrational Coordinates with Polarization-Selective Two-Dimensional Vibrational-Electronic Spectroscopy. *J. Phys. Chem. Lett.* **2020**, *11*, 1558−1563.
(17) Wu, E. C.; Ge, Q.; Arsenault, E. A.; Lewis, N. H. C.; Gruenke, N. L.; Head-Gordon, M. J.; Fleming, G. R. Two-Dimensional Electronic-Vibrational Spectroscopic Study of Conical Intersection Dynamics: An Experimental and Electronic Structure Study. *Phys. Chem. Chem. Phys.* **2019**, *21*, 14153−14163.
(18) Huang, J. Y.; Shen, Y. R. Theory of Doubly Resonant Infrared-Visible Sum-Frequency and Difference-Frequency Generation from Adsorbed Molecules. *Phys. Rev. A: At., Mol., Opt. Phys.* **1994**, *49*, 3973−3981.
(19) Raschke, M. B.; Hayashi, M.; Lin, S. H.; Shen, Y. R. Doubly-Resonant Sum-Frequency Generation Spectroscopy for Surface Studies. *Chem. Phys. Lett.* **2002**, *359*, 367−372.
(20) Hayashi, M.; Lin, S. H.; Raschke, M. B.; Shen, Y. R. A Molecular Theory for Doubly Resonant Ir−Uv-Vis Sum-Frequency Generation. *J. Phys. Chem. A* **2002**, *106*, 2271−2282.
(21) Wu, D.; Deng, G.-H.; Guo, Y.; Wang, H.-f. Observation of the Interference between the Intramolecular Ir−Visible and Visible−Ir Processes in the Doubly Resonant Sum Frequency Generation Vibrational Spectroscopy of Rhodamine 6g Adsorbed at the Air/Water Interface. *J. Phys. Chem. A* **2009**, *113*, 6058−6063.
(22) Rao, Y.; Turro, N. J.; Eisenthal, K. B. Solvation Dynamics at the Air/Water Interface with Time-Resolved Sum-Frequency Generation. *J. Phys. Chem. C* **2010**, *114*, 17703−17708.
(23) Bozzini, B.; D'Urzo, L.; Mele, C.; Busson, B.; Humbert, C.; Tadjeddine, A. Doubly Resonant Sum Frequency Generation Spectroscopy of Adsorbates at an Electrochemical Interface. *J. Phys. Chem. C* **2008**, *112*, 11791−11795.
(24) Belkin, M. A.; Shen, Y. R. Doubly Resonant Ir-Uv Sum-Frequency Vibrational Spectroscopy on Molecular Chirality. *Phys. Rev. Lett.* **2003**, *91*, 213907.
(25) Han, S. H.; Ji, N.; Belkin, M. A.; Shen, Y. R. Sum-Frequency Spectroscopy of Electronic Resonances on a Chiral Surface Monolayer of Bi-Naphthol. *Phys. Rev. B: Condens. Matter Mater. Phys.* **2002**, *66*, 165415.
(26) Chou, K. C.; Westerberg, S.; Shen, Y. R.; Ross, P. N.; Somorjai, G. A. Probing the Charge-Transfer State of Co on Pt(111) by Two-Dimensional Infrared-Visible Sum Frequency Generation Spectroscopy. *Phys. Rev. B: Condens. Matter Mater. Phys.* **2004**, *69*, 153413.
(27) Sengupta, S.; Bromley III, L.; Velarde, L. Aggregated States of Chalcogenorhodamine Dyes on Nanocrystalline Titania Revealed by Doubly Resonant Sum Frequency Spectroscopy. *J. Phys. Chem. C* **2017**, *121*, 3424−3436.
(28) Busson, B.; Farhat, M.; Nini Teunda, P. J.; Roy, S.; Jarisz, T.; Hore, D. K. All-Experimental Analysis of Doubly Resonant Sum-Frequency Generation Spectra: Application to Aggregated Rhodamine Films. *J. Chem. Phys.* **2021**, *154*, 224704.
(29) Elsenbeck, D.; Das, S. K.; Velarde, L. Substrate Influence on the Interlayer Electron−Phonon Couplings in Fullerene Films Probed with Doubly-Resonant Sfg Spectroscopy. *Phys. Chem. Chem. Phys.* **2017**, *19*, 18519−18528.
(30) Wang, J.; Wu, X.; He, Y.; Guo, W.; Zhang, Q.; Wang, Y.; Wang, Z. Investigation of the Electronic Structure of Cds Nanoparticles with Sum Frequency Generation and Photoluminescence Spectroscopy. *J. Phys. Chem. C* **2019**, *123*, 27712−27716.
(31) Busson, B. Doubly Resonant Sfg and Dfg Spectroscopies: An Analytic Model for Data Analysis Including Distorted and Rotated Vibronic Levels. I. Theory. *J. Chem. Phys.* **2020**, *153*, 174701.
(32) Busson, B. Doubly Resonant Sfg and Dfg Spectroscopies: An Analytic Model for Data Analysis Including Distorted and Rotated Vibronic Levels. Ii. Applications. *J. Chem. Phys.* **2020**, *153*, 174702.
(33) Busson, B. All-Experimental Analysis of Doubly Resonant Sum-Frequency Generation Spectra for Franck−Condon and Herzberg−Teller Vibronic Modes. *J. Chem. Phys.* **2022**, *156*, 204704.
(34) Yang, S.; Noguchi, H.; Uosaki, K. Electronic Structure of the Co/Pt(111) Electrode Interface Probed by Potential-Dependent Ir/Visible Double Resonance Sum Frequency Generation Spectroscopy. *J. Phys. Chem. C* **2015**, *119*, 26056−26063.
(35) McGuire, J. A.; Shen, Y. R. Ultrafast Vibrational Dynamics at Water Interfaces. *Science* **2006**, *313*, 1945−1948.
(36) Bredenbeck, J.; Ghosh, A.; Smits, M.; Bonn, M. Ultrafast Two Dimensional-Infrared Spectroscopy of a Molecular Monolayer. *J. Am. Chem. Soc.* **2008**, *130*, 2152−2153.
(37) Xiong, W.; Laaser, J. E.; Mehlenbacher, R. D.; Zanni, M. T. Adding a Dimension to the Infrared Spectra of Interfaces Using Heterodyne Detected 2d Sum-Frequency Generation (Hd-2d-Sfg) Spectroscopy. *Proc. Natl. Acad. Sci.* **2011**, *108*, 20902−20907.
(38) Singh, P. C.; Nihonyanagi, S.; Yamaguchi, S.; Tahara, T. Ultrafast Vibrational Dynamics of Water at a Charged Interface Revealed by Two-Dimensional Heterodyne-Detected Vibrational Sum Frequency Generation. *J. Chem. Phys.* **2012**, *137*, 094706.
(39) Wang, J.; Clark, M. L.; Li, Y.; Kaslan, C. L.; Kubiak, C. P.; Xiong, W. Short-Range Catalyst−Surface Interactions Revealed by Heterodyne Two-Dimensional Sum Frequency Generation Spectroscopy. *J. Phys. Chem. Lett.* **2015**, *6*, 4204−4209.
(40) Vanselous, H.; Stingel, A. M.; Petersen, P. B. Interferometric 2d Sum Frequency Generation Spectroscopy Reveals Structural Heterogeneity of Catalytic Monolayers on Transparent Materials. *J. Phys. Chem. Lett.* **2017**, *8*, 825−830.
(41) Schleeger, M.; Grechko, M.; Bonn, M. Background-Free Fourth-Order Sum Frequency Generation Spectroscopy. *J. Phys. Chem. Lett.* **2015**, *6*, 2114−2120.
(42) Deng, G.-H.; Qian, Y.; Wei, Q.; Zhang, T.; Rao, Y. Interface-Specific Two-Dimensional Electronic Sum Frequency Generation Spectroscopy. *J. Phys. Chem. Lett.* **2020**, *11*, 1738−1745.
(43) Deng, G. H.; Wei, Q.; Qian, Y.; Zhang, T.; Leng, X.; Rao, Y. Development of Interface-/Surface-Specific Two-Dimensional Electronic Spectroscopy. *Rev. Sci. Instrum.* **2021**, *92*, 023104.
(44) Deng, G. H.; Qian, Y.; Zhang, T.; Han, J.; Chen, H.; Rao, Y. Two-Dimensional Electronic-Vibrational Sum Frequency Spectroscopy for Interactions of Electronic and Nuclear Motions at Interfaces. *Proc. Natl. Acad. Sci. U. S. A.* **2021**, *118*, No. e2100608118.
(45) Brida, D.; Manzoni, C.; Cerullo, G. Phase-Locked Pulses for Two-Dimensional Spectroscopy by a Birefringent Delay Line. *Opt. Lett.* **2012**, *37*, 3027−3029.
(46) Réhault, J.; Maiuri, M.; Oriana, A.; Cerullo, G. Two-Dimensional Electronic Spectroscopy with Birefringent Wedges. *Rev. Sci. Instrum.* **2014**, *85*, 123107.
(47) Deng, G. H.; Qian, Y.; Rao, Y. Development of Ultrafast Broadband Electronic Sum Frequency Generation for Charge Dynamics at Surfaces and Interfaces. *J. Chem. Phys.* **2019**, *150*, 024708.
(48) Zhang, T.; Huangfu, Z.-C.; Qian, Y.; Lu, Z.; Gao, H.; Rao, Y. Spectral Phase Measurements of Heterodyne Detection in Interfacial Broadband Electronic Spectroscopy. *J. Phys. Chem. C* **2022**, *126*, 2823−2832.
(49) Rao, Y.; Xu, M.; Jockusch, S.; Turro, N. J.; Eisenthal, K. B. Dynamics of Excited State Electron Transfer at a Liquid Interface

https://doi.org/10.1021/jacsau.3c00074
JACS Au 2023, 3, 1413−1423

Using Time-Resolved Sum Frequency Generation. *Chem. Phys. Lett.* **2012**, *544*, 1−6.
(50) Rao, Y.; Qian, Y.; Deng, G. H.; Kinross, A.; Turro, N. J.; Eisenthal, K. B. Molecular Rotation in 3 Dimensions at an Air/Water Interface Using Femtosecond Time Resolved Sum Frequency Generation. *J. Chem. Phys.* **2019**, *150*, 094709.
(51) Hättig, C.; Weigend, F. Cc2 Excitation Energy Calculations on Large Molecules Using the Resolution of the Identity Approximation. *J. Chem. Phys.* **2000**, *113*, 5154−5161.
(52) Dunning, T. H. Gaussian Basis Sets for Use in Correlated Molecular Calculations. I. The Atoms Boron through Neon and Hydrogen. *J. Chem. Phys.* **1989**, *90*, 1007−1023.
(53) Wyczalkowski, M. A.; Vitalis, A.; Pappu, R. V. New Estimators for Calculating Solvation Entropy and Enthalpy and Comparative Assessments of Their Accuracy and Precision. *J. Phys. Chem. B* **2010**, *114*, 8166−8180.
(54) Bayly, C. I.; Cieplak, P.; Cornell, W.; Kollman, P. A. A Well-Behaved Electrostatic Potential Based Method Using Charge Restraints for Deriving Atomic Charges: The Resp Model. *J. Phys. Chem.* **1993**, *97*, 10269−10280.
(55) Wang, J.; Wolf, R. M.; Caldwell, J. W.; Kollman, P. A.; Case, D. A. Development and Testing of a General Amber Force Field. *J. Comput. Chem.* **2004**, *25*, 1157−1174.
(56) Wu, Y.; Tepper, H. L.; Voth, G. A. Flexible Simple Point-Charge Water Model with Improved Liquid-State Properties. *J. Chem. Phys.* **2006**, *124*, 024503.
(57) Ahlrichs, R.; Bär, M.; Häser, M.; Horn, H.; Kölmel, C. Electronic Structure Calculations on Workstation Computers: The Program System Turbomole. *Chem. Phys. Lett.* **1989**, *162*, 165−169.
(58) Kühne, T. D.; Iannuzzi, M.; Del Ben, M.; Rybkin, V. V.; Seewald, P.; Stein, F.; Laino, T.; Khaliullin, R. Z.; Schütt, O.; Schiffmann, F.; et al. Cp2k: An Electronic Structure and Molecular Dynamics Software Package - Quickstep: Efficient and Accurate Electronic Structure Calculations. *J. Chem. Phys.* **2020**, *152*, 194103.
(59) Khalil, M.; Demirdoven, N.; Tokmakoff, A. Obtaining Absorptive Line Shapes in Two-Dimensional Infrared Vibrational Correlation Spectra. *Phys. Rev. Lett.* **2003**, *90*, 047401.
(60) Hamm, P.; Zanni, M. *Concepts and Methods of 2d Infrared Spectroscopy*; Cambridge University Press, 2011; p 298.
(61) Qian, Y.; Deng, G.-h.; Rao, Y. In Situ Spectroscopic Probing of Polarity and Molecular Configuration at Aerosol Particle Surfaces. *J. Phys. Chem. Lett.* **2020**, *11*, 6763−6771.
(62) Lueck, H. B.; Daniel, D. C.; McHale, J. L. Resonance Raman Study of Solvent Effects on a Series of Triarylmethane Dyes. *J. Raman Spectrosc.* **1993**, *24*, 363−370.
(63) Gaynor, J. D.; Khalil, M. Signatures of Vibronic Coupling in Two-Dimensional Electronic-Vibrational and Vibrational-Electronic Spectroscopies. *J. Chem. Phys.* **2017**, *147*, 094202.
(64) Rao, Y.; Tao, Y.-s.; Wang, H.-f. Quantitative Analysis of Orientational Order in the Molecular Monolayer by Surface Second Harmonic Generation. *J. Chem. Phys.* **2003**, *119*, 5226−5236.
(65) Rao, Y.; Hong, S.-Y.; Turro, N. J.; Eisenthal, K. B. Molecular Orientational Distribution at Interfaces Using Second Harmonic Generation. *J. Phys. Chem. C* **2011**, *115*, 11678−11683.
(66) Fita, P.; Punzi, A.; Vauthey, E. Local Viscosity of Binary Water +Glycerol Mixtures at Liquid/Liquid Interfaces Probed by Time-Resolved Surface Second Harmonic Generation. *J. Phys. Chem. C* **2009**, *113*, 20705−20712.

https://doi.org/10.1021/jacsau.3c00074
JACS Au 2023, 3, 1413−1423